A Joint Experimental and Theoretical Study on the Nanomorphology of CaWO4 Crystals

ARTICLE *in* THE JOURNAL OF PHYSICAL CHEMISTRY C · OCTOBER 2011

Impact Factor: 4.77 · DOI: 10.1021/jp205764s

THE JOURNAL OF PHYSICAL CHEMISTRY C

ARTICLE

pubs.acs.org/JPCC

A Joint Experimental and Theoretical Study on the Nanomorphology of $CaWO_4$ Crystals

Valéria M. Longo,[†] Lourdes Gracia,[*,‡] Daniel G. Stroppa,[§] Laécio S. Cavalcante,[†] Marcelo Orlandi,[†] Antônio J. Ramirez,[§] Edson R. Leite,[†] Juan Andrés,[*,‡] Armando Beltrán,[‡] José A. Varela,[†] and Elson Longo[†]

[†]LIEC, Instituto de Química, UNESP, P.O. Box 355, 14800-900, Araraquara, Brazil

[‡]MALTA Consolider Team, Departament de Química Física i Analítica, Universitat Jaume I, Campus de Riu Sec, Castello, E12080, Spain

[§]Brazilian Nanotechnology National Laboratory, 13083-970 Campinas, SP, Brazil

ABSTRACT: By the joint use of experimental techniques such as field emission scanning electron microscopy (FEG-SEM), transmission electron microscopy (TEM), and high resolution transmission electron microscopy (HR-TEM) and ab initio theoretical calculations on the slabs surface energy with application of the Wulff construction was performed to study the shape of $CaWO_4$ nanocrystals obtained by a microwave assisted hydrothermal (MAH) method. Under equilibrium conditions, the shape is a slightly truncated tetragonal bipyramid enclosed with eight isosceles trapezoidal surfaces of (101) (Ca-terminated) and two top squares of (001) (O-terminated). Calculated band structures and densities of states are analyzed to find the electronic structures of the different surfaces. The more pronounced elongation of the (001) facet of the experimental FIG with respect to the theoretical prediction results from the favorable interaction between hydroxyl anions and Ca exposed atoms of this surface.

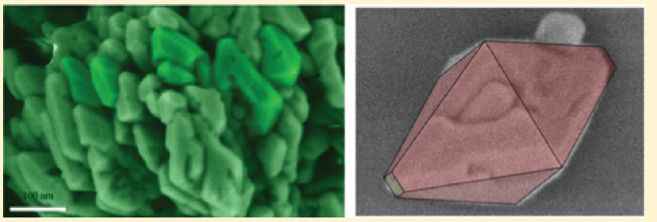

1. INTRODUCTION

The controllable fabrication of inorganic materials with desired morphologies, architectures, and properties at micro- and nanoscale levels is a key challenge in materials science.[1] Many applications such as heterogeneous catalysis, gas sensing, energy conversion, and storage are very sensitive to surface atomic structures. This fact is even more important for nanostructured materials where the surface energy contributes significantly to the total energy. Considerable progress could be made in the field of nanoscience if faceted nanoparticles could be described in accurate detail[2] because the anomalous surface energy of nanostructures induces many novel nanosized-effects and provides technological potentials.

Knowledge about the surface structures and energies facilitates the prediction and optimization regarding the syntheses and eventually the processing of nanocrystals into genuine nanomaterials. The evolution of a crystal shape during growth is basically driven by continuously decreasing the total surface energy of the crystal and finally stops at the minimum surface energy point in a given growth environment. When a crystal grows, different facets grow with different rates. High-energy facets typically have higher growth rates than low-energy facets. Overall, the final crystal shape is dominated by the slow-growth facets that have low surface energy.

Nanomorphology is dictated by a complex interplay of relative rates of atom attachment on different crystallographic facets of nanocrystals that depend on externally tunable parameters such as temperature and the presence of adsorbates/capping agents. Therefore, these predicted shapes are definitely derived to some extent from the observed morphologies of natural or synthetic crystals influenced by the environmental growth conditions. Several insightful researchers have reported experimental and theoretical aspects of crystal shape engineering.[2−9] Recently, Barnard et al.[2,10] reviewed the theoretical and computational approaches to morphology and evolution, which they applied to the study of the structure and formation of discrete inorganic nanoparticles.

Materials that are not fully periodic (e.g., nanocrystals) require experimental approaches that can tackle the structural issues to a high degree of accuracy. In the case of nanometric-sized particles, measurements are more problematic due to limited imaging techniques and to the process of coalescence between nanoparticles. Therefore, the experimental determination of the surface energy of crystals is a very challenging task, and the principal difficulty with the application of these methods to solving the nanostructure problem is that, in general, any one technique does not contain sufficient information to constrain a unique structural solution. For this type of study, the use of precise experimental and theoretical techniques experimentally is imperative.[11]

Recently, a detailed characterization of the anomalous oriented attachment behavior for SnO_2 nanocrystals was achieved.[12] The assemblies from SnO_2 building blocks are being widely investigated due to their unique properties of 3D micro-/nanostructures built up via self-assembly. These structures are composed of nanoscaled building blocks, while the total size is in the micrometer scale. The cooperation of the micro- and

Received: June 20, 2011
Revised: July 26, 2011
Published: August 02, 2011

nanostructure in such a hierarchical system provides a new approach to elicit new properties. In addition, we have reported a novel approach to morphological prediction by combining high-resolution transmission electron microscopy (HRTEM) characterization and surface ab initio calculation for SnO_2:Sb.[13] In this work, we demonstrate the ability of this strategy to investigate the nanomorphology of $CaWO_4$ nanocrystals synthetized by a MAH route. The growth mechanism is discussed, and the physical properties of the product (i.e., band structure and optical properties) were also studied. By using systematic experimental techniques such as field emission scanning electron microscopy (FEG-SEM), transmission electron microscopy (TEM), HRTEM, and theoretical surface ab initio calculations applied to the Wulff construction, as-prepared $CaWO_4$ nanocrystals were investigated. Band structures and density of states were analyzed in detail to find a nanoscale electronic structure −property correlation, which will provide some significant perspectives regarding future directions.

2. EXPERIMENTAL SECTION

A variety of synthetic methods yield well-defined and high-purity $CaWO_4$ nanoparticles with different sizes and shapes by carefully controlling the crystallization morphology.[14−28] $CaWO_4$ powders obtained by coprecipitation were processed using a MAH method in the presence of polyethylene glycol (PEG), which promotes faster reaction rates and shorter reaction times and thereby leads to an overall reduction in energy consumption.[29]

Along with higher product yields and improved chemical selectivity, these attributes make microwave assisted techniques inherently green as compared to conventional heating techniques. In addition, this method offers flexibility in terms of controlling particle size, shape, and surface chemistry. The combination of liquid-phase synthesis with the MAH route is an appropriate tool to control morphological properties of nanomaterials, in particular, metal oxide nanoparticles.[30] Our group has employed various efforts to demonstrate that this method is one of the most versatile ways to obtain crystalline, micro-, and/or nanoscale particles.[31−34] In this rapidly developing area of research, recently, Bilecka and Niederberger[35] have published an overview of MAH liquid-phase routes to obtain inorganic nanomaterials.

The typical synthesis procedure is described as follows: 5×10^{-3} mol of tungstic acid (H_2WO_4) (99% purity, Aldrich), 5×10^{-3} mol of calcium acetate monohydrate [$Ca(CH_3CO_2)_2 \cdot H_2O$] (99.5% purity, Aldrich), and 0.1 g of PEG (M_w 200) (99.9% purity, Aldrich) were dissolved in 100 mL of deionized water. Next, 5 mL of ammonium hydroxide (NH_4OH) (30% in NH_3, Synth) was added in the solution until the pH value reached 10. The aqueous solution was then placed in an ultrasound for 30 min at room temperature. Next, the mixture was transferred into a Teflon autoclave, which was sealed and placed into a MAH system (2.45 GHz, maximum power of 800 W). MAH temperatures were kept at 140 °C for 30 min using a heating rate fixed at 25 °C/min. The pressure into the autoclave was stabilized at 294 kPa. After the MAH treatment, the autoclave was cooled to room temperature. The resulting solution was washed with deionized water several times to neutralize the pH of the solution (∼7), and the white precipitates were finally collected. Using the same experimental conditions, the powders obtained were dried in a conventional furnace at 70 °C for 10 h. Four samples of $CaWO_4$ powders were prepared to analyze the reproducibility of the method.

$CaWO_4$ nanostructures were characterized by different techniques. X-ray diffraction (XRD) was carried out on the as-prepared sample, and the corresponding measurements were obtained (Rigaku DMax 2500PC). The morphology and size of the products are investigated by using FE-SEM (Jeol JSM 6330F) and TEM (Jeol 3010). The growth directions of $CaWO_4$ nanooctahedra were estimated using selected-area electron diffraction (SAED) and HRTEM.

3. THEORETICAL SECTION

Surface energy calculations for $CaWO_4$ nanocrystals were performed with a CRYSTAL06[36] program package. Tungsten, calcium and oxygen centers have been described by a PS-11d3G, 86-511d3G, and O (6-31d1G) basis set, respectively, which was taken from the Crystal website.[37] Becke's three-parameter hybrid nonlocal exchange functional[38] combined with a Lee−Yang−Parr gradient-corrected correlation functional (B3LYP)[39] was used. Diagonalization of the Fock matrix was performed at adequate *k*-points grids in the reciprocal space. The thresholds controlling the accuracy of the calculation of Coulomb and exchange integrals were set to 10^{-8} (ITOL1 to ITOL4) and 10^{-14} (ITOL5), whereas the percent of Fock/Kohn−Sham matrices mixing was set to 40 (IPMIX = 40).[36]

The scheelite-type $CaWO_4$ has a tetragonal structure with space group ($I4_1/a$). The calcium ions are 8-fold coordinated with the oxygen's atoms surrounding tungstate groups. The tungsten atoms are tetrahedrally coordinated with the oxygen's atoms, where the tetrahedral angles are slightly distorted. Full optimization of the cell parameters (*a* and *c*) and the internal atomic position for the bulk of $CaWO_4$ were carried out. The low index (110), (101), (100), (001), (111), and (103) surfaces were modeled by unreconstructed (truncated bulk) slab models by using calculated equilibrium geometry. Because these surfaces have a different number of atoms in each layer to reach the symmetry and stoichiometry, the low-index surfaces were modeled with different thicknesses in the *z*-direction but were periodic in the *x*- and *y*-directions. After the corresponding convergence test on the systems, slab models containing 20, 38, 15, 15, 45, and 36 atomic layers for the (110), (101), (100), (001), (111), and (103) surfaces, respectively, were selected. For the models used here, the bottom and top planes were equivalent in symmetry. A complete relaxation in each model was performed. The band structures of the main $CaWO_4$ surfaces were constructed along the appropriate high-symmetry directions of the corresponding irreducible Brillouin zones.

It is well-known that Wulff[40] construction is a standard method for determining the equilibrium shape of bulk crystals. The underlying basis for these size- and shape-dependent thermodynamic constructions[40] states that the equilibrium shape of macroscopic crystals can be found by minimizing the surface energies with respect to a fixed volume[41] as discussed in detail by Herring.[42]

The energy of the terminated surface of a solid material is always higher than the energy of the bulk, and this energy difference is defined as the surface energy. On the basis of the surface energies of all facets, the Wulff construction can be used to determine the equilibrium morphology of a material.

Surface energy minimization is the central standard to optimize the composition of the crystal surface. Sun[43,44] has shown that the size-induced change of quantities such as surface energy

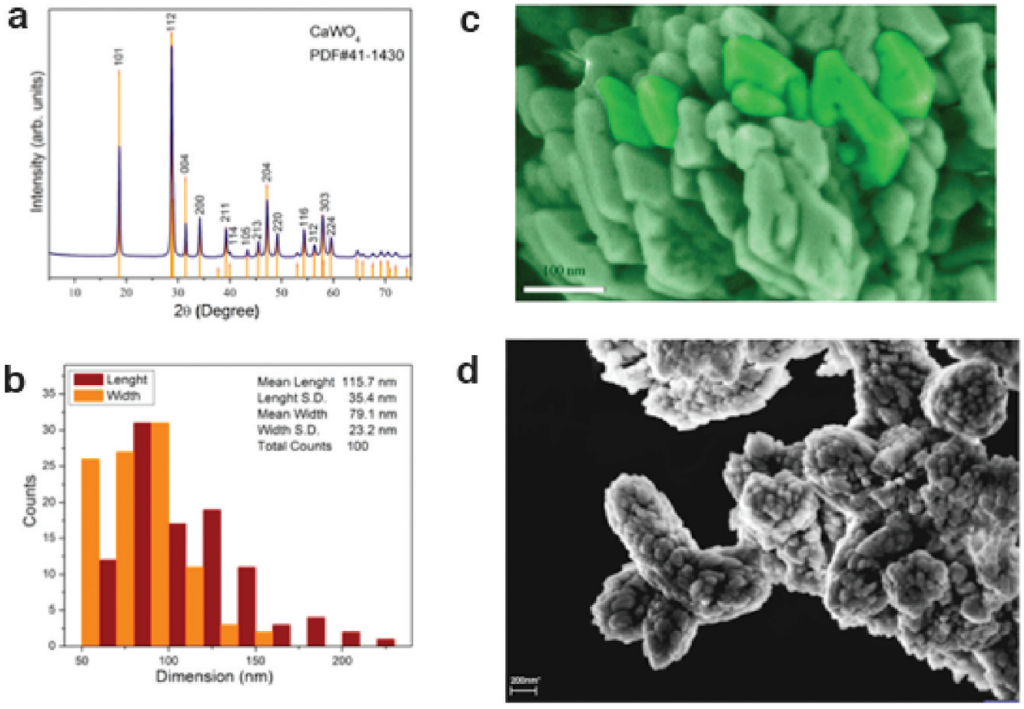

Figure 1. (a) XRD pattern of $CaWO_4$ nano-octahedrons with a CIF number 15.586. (b) Size distribution histogram where the red and orange bars represent the length and width, respectively. The inset text indicates the mean sizes with their respective standard deviations for a total count of 100 particles. (c) Typical FEG-SEM images of $CaWO_4$ nano-octahedra with a self-organization. (d) Extended FEG-SEM image morphologies indicating peanut-like nanoparticles.

is interdependent and arises from the same origin as the atomic undercoordination, and the surface energy increases with increasing density of dangling bonds. The surface relative energy variations can basically be explained by the different chemical compositions of the facets, which result in diverse degrees of broken chemical bonds on the surface[45] and sites therein. The shorter and stronger bonds in the surface skin (up to two or three atomic layers) dominate the size dependency, while bonds in the core interior remain their bulk nature.[46]

Wulff[40,41,47] construction was applied to build theoretical crystals by using the ab initio calculated surface energies and the $CaWO_4$ $I4_1/a$ crystal structure. Surface energy, E_{surf}, is defined as the total energy per repeating cell of the slab minus the total energy of the same number of atoms of the perfect crystal divided by the surface area per repeating cell of the two sides of the slab, that is, $E_{surf} = (E_{slab} - nE_{bulk})/2A$. This equation has been used by us in previous studies.[13,48]

4. RESULTS AND DISCUSSION

XRD patterns of synthesized $CaWO_4$ indicated highly crystalline single phase nanocrystals with a scheelite-type tetragonal structure and a space group $I4_1/a$ in a C_{4h}^6 symmetry (JCPDS number 41-1430) (see Figure 1a). An image analysis of 100 particles of FEG-SEM micrographs (obtained using ImageJ software (http://rsbweb.nih.gov/ij/)) is presented in Figure 1b and shows that the average particle size distribution of nano-octahedra crystals has a mean length of 115.7 nm and a mean width of 79.1 nm. FEG-SEM micrographs (see Figure 1c) show that nanocrystalline structures have octahedra-like morphology with different sizes. These morphologies are formed by an oriented attachment (OA) mechanism, which has previously been observed for materials with a scheelite-type structure.[49−53] In this nonclassical crystallization process, the formation of a crystal controlled by a monomer-by-monomer assembly is replaced by a process involving the spontaneous self-organization of adjacent nanocrystals to share a common crystallographic orientation and coalescence, that is, by the OA growth mechanism.[3,48,54] A kinetic model to describe the OA growth process of nanoparticles in colloidal suspensions has been suggested,[55] and posterior studies based on this mechanism have been developed by Penn[56] and Xu et al.[57] Therefore, scheelite-type structures tend to be faceted and aligned by "docking" processes involving crystallographic fusion between some faces with lower surface energy because they are more abundant and generate an extended morphology. These extended morphologies, which are derived by oriented nanoparticles, are peanut-like in the range of a few micrometers (Figure 1d).

Figures 2a−c displays FEG-SEM images of an individual $CaWO_4$ nano-octahedron, the geometric construction, and the superimposition of the experimental and geometric image, respectively. The crystal shape in Figure 2b was geometrically constructed on the basis of the crystallographic tetragonal structure with a space group $I4_1/a$, and the shape was adjusted as a function of FEG-SEM micrographs (Figure 2a). A remarkable agreement between the superimposed images can be observed in Figure 2c. However, according to the geometric construction, there are two ways in which the facets can be indexed: by the {101} and {001} family or by the {111} and {001} family.

The electronic structure of $CaWO_4$ and their surfaces have scarcely been studied. Table 1 presents the calculated surface

energies values (E_{surf}) for (001), (100), (110), (101), (103), and (111) planes, the number of $CaWO_4$ layers of each surface model, and their calculated surface energy. On the basis of DFT calculations, the (101) facet with a surface energy of 0.76 J m^{-2} was chosen instead of the (111) facet with a surface energy of 2.98 J m^{-2}. Cooper et al.[58] have employed electronic structure calculations based on the density functional theory and atomistic simulations to investigate the geometry and electronic structure of the perfect crystal, and to calculate the process of incorporating water into the bulk material. These authors identified the {001} and {101} families of dry $CaWO_4$ to be the most stable due to the combination of relative high coordination numbers of the surface species and large interlayer spacing. However, in their calculations, the morphology was also dominated by the {111} families (with a surface energy of only 0.1 and 0.15 eV higher than {001} and {101}, respectively), which presented a different aspect as compared to this work.

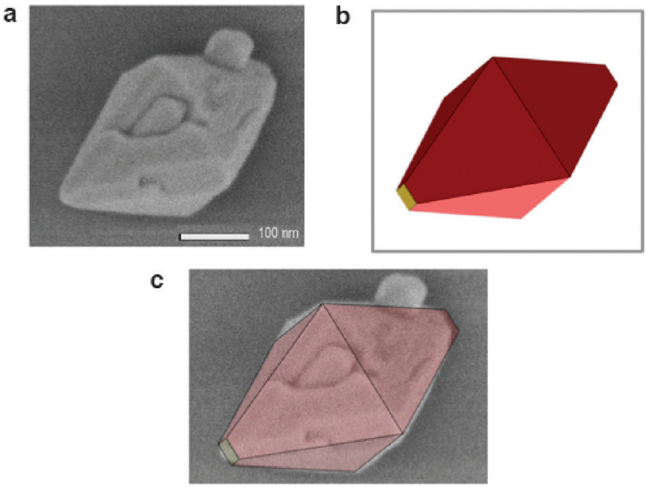

Figure 2. (a) FEG-SEM image of an individual $CaWO_4$ nano-octahedron; (b) the geometric construction; and (c) superimposed experimental and calculated images.

Table 1. Number of $CaWO_4$ Units, Area, Surface Energy, Band Gap Energy, and Fermi Energy (E_f) for (001), (100), (110), (101), (103), and (111) Surfaces of $CaWO_4$[a]

$CaWO_4$	n	area (Å^2)	E_{surf} (J m^{-2})	band gap (eV)	E_f (eV)
bulk	2			5.69	−4.26
(001)	5	27.05	0.67	5.64	−7.37
(100)	6	58.74	1.19	4.61	−6.77
(110)	4	41.53	1.39	5.70	−6.40
(101)	6	32.33	0.76	5.85	−5.95
(103)	6	50.08	1.85	4.19	−6.31
(111)	9	87.36	2.98	0.56	−0.93

[a] All surfaces are O-terminated except (101), which is Ca-terminated.

The ab initio calculated surface energy values for different crystalline planes are listed in Figure 3 along with the resulting Wulff construction derived from theoretical results and FEG-SEM images. The shape under equilibrium conditions is a slightly truncated tetragonal bipyramid enclosed with the eight isosceles trapezoidal surfaces of (101) and two top squares of (001) (see Figure 3); the percentage of (101) is predicted to be as high as 98%. A comparison and analysis of both images show that the morphology from FEG-SEM data is more elongated along the [001] direction than the theoretical morphology. Despite some differences between the vacuo conditions used in the calculations and the real conditions for crystal growth, the most stable facets predicted usually show the largest fraction of crystal surfaces.

At this stage, it is important to note that a number of questions are unanswered. It should be kept in mind that the above equilibrium shape calculations are conducted in vacuo at absolute zero temperature, which is clearly different from the actual conditions. In fact, environment can change the relative stability of different facets. The interaction with the solvent, surfactant, and ionic species involved in the syntheses of $CaWO_4$ can play a role, which was not considered in the present ab initio calculations. Different surface structures interacting with their surroundings can change the value of its surface energy and modify their final morphology.

A theoretical analysis is aimed at studying the electronic structure of the (101) (Ca-terminated) and (001) (O-terminated) facets. In Figure 4, we show the electronic charge density contours in these surfaces, and the analysis of the results points out that the majority of charges are positioned on O centers and the distribution of electronic charge is spherical, which results in the bonding between O−Ca or O−W atoms. This behavior can be associated with the ionic character of these types of interactions due to the large electronegativity difference between O (3.5) and Ca (1.3) or W (1.7) atoms. The net Mulliken charge values for the superficial O and Ca atoms at both (001) and (101) surfaces are −1.26e, +1.61e, and −1.29e, +1.62e, respectively. Therefore, O-terminated facets offer a negative electronic charge to the surroundings, while Ca-terminated facets present a positive character.

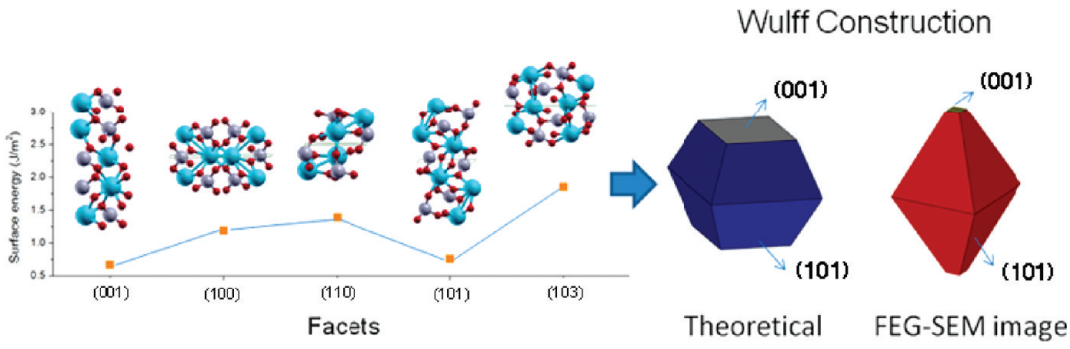

Figure 3. Ab initio calculated surface energies for different crystallographic planes (Ca atoms in blue, W atoms in gray, and O atoms in red), Wulff constructed nanocrystal, and geometric FEG-SEM image. The resulting facets of Wulff crystal and FEG-SEM images are indicated as (001) and (101).

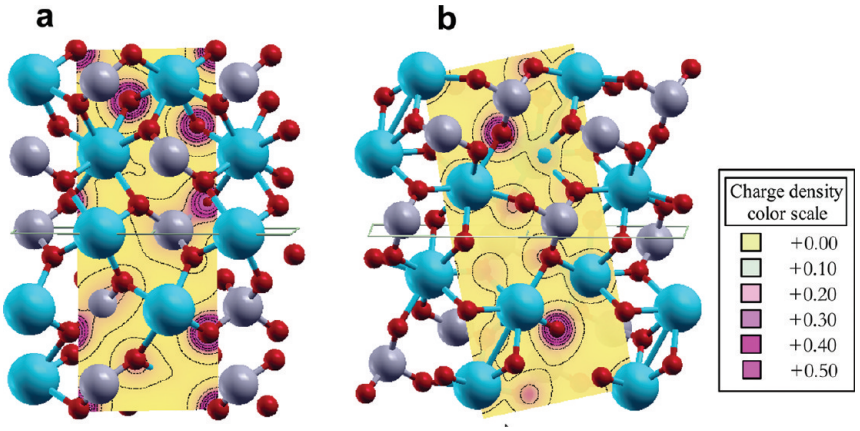

Figure 4. Total charge density projected on the plane containing the (a) O-terminated (001) facet; and (b) the Ca-terminated (101) facet. Ca atoms in blue, W atoms in gray, and O atoms in red.

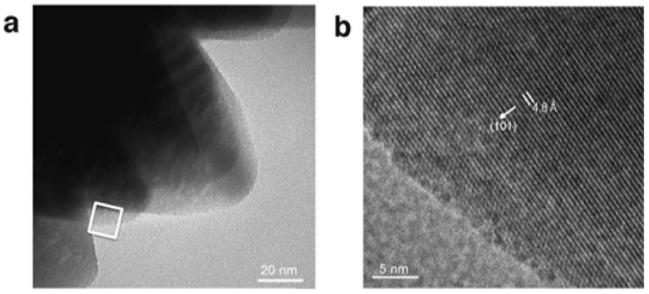

Figure 5. (a) TEM micrograph of faceted $CaWO_4$ in the same crystallographic orientation; and (b) HRTEM image of the interplanar distance of 4.8 Å that corresponds to the (101) plane.

With the synthesis procedure, $CaWO_4$ crystals are subjected to alkaline conditions (pH = 10). The above information supports the conclusion that the presence of hydroxyl anions favors the formation of Ca−OH^- bonding interactions at the surface, which leads to a decrease in the (101) (Ca-terminated) surface energy resulting in more stability than the (001) surface (O-terminated) because of the positive charge nature of the former in relation to the negative behavior of the latter. This fact confirms that (101) facets are more stabilized in the real condition and justifies the discrepancies between experimental and theoretical results. In this respect, it is important to cite the work of Barnard and Curtiss[59] on the nanomorphologies of anatase and rutile nanoparticles; on the basis of surface free energies and surface tensions from first-principles calculations, these authors systematically studied the effects of surface chemistry in terms of acidic and alkaline conditions. The surface termination by hydrogen (acidic conditions) results in little change in the shapes of both polymorphs relative to vacuo. However, in water-terminated surfaces and hydrogen-poor surfaces (in particular oxygenated surfaces), both polymorphs are apparently elongated.

This argument can also be used to discuss the OA mechanism. This process is controlled by different factors: The first factor is associated with the percentage of exposed facets because more abundant facets with a high superficial area are more susceptive to aggregation. In addition, different facets have different polarizations that can change when they interact with the solvent. Particularly, in the case of the $CaWO_4$, the formation of the (001) facet (corresponding to O-terminated) has a thermodynamically smaller superficial area than expected. Therefore, more atoms are defunded to the (001) facet after nucleation, and the solvent (in this case water) interacts more effectively with the (101) facet and reduces its surface energy.

To show that our faceting prediction proposition is correct, TEM and HRTEM analyses were conducted; the resulting images are depicted in Figure 5. As can be observed, $CaWO_4$ particle facets are quite similar (Figure 5a). From the analysis of an expanded HRTEM image (Figure 5b), it is clear that the interplanar distance of this nanocrystal is about 4.8 Å, which is related to the (101) crystallographic planes of $CaWO_4$ scheelite with a tetrahedral structure as observed by XRD data (Figure 1a).

An analysis of the results depicted in Figures 1b and 2a points out that $CaWO_4$ nanoparticles join together in the OA process by (101) planes, which results in peanut-like structures in the range of a few micrometers. In the nanocrystal structure, more than 98% of the total area corresponds to (101) facets. In each facet, the energy was calculated for the Fermi level (E_f). Overall, these results show a considerable spread in the values of E_f as the facet changes. The variations in the energy of the Fermi level are of particular interest, because aligning this value with other electronic materials is important in designing new devices.[60] However, if we examine the results for particular crystallographic facets, we find that the energy of the Fermi level is independent of the facet.

The differences in the electronic structure are discussed by analyzing the (001) and (101) facets that compose the surface of the $CaWO_4$ nano-octahedra. Figure 6a and b depicts the calculated band structure and densities of state projected on atoms and the main corresponding orbitals of (001) and (101) facets, respectively. The top of the valence band (VB) as well as the bottom of the conduction band (CB) are at the Γ point; thus, the band gap is direct. The minimum calculated direct gap is 5.64 eV, for the (001) facet that is close to the 5.69 eV bulk value, while a value of 5.85 eV is found for the gap of the (101) facet.

For both surfaces, the valence bands are composed of 2p orbitals of O atoms but with a major $2p_z$ contribution in (001) and a $2p_x$ contribution in (101). The first conduction band shows many differences between O-terminated (001) and Ca-terminated (101) facets. The O-terminated facet with a broadened

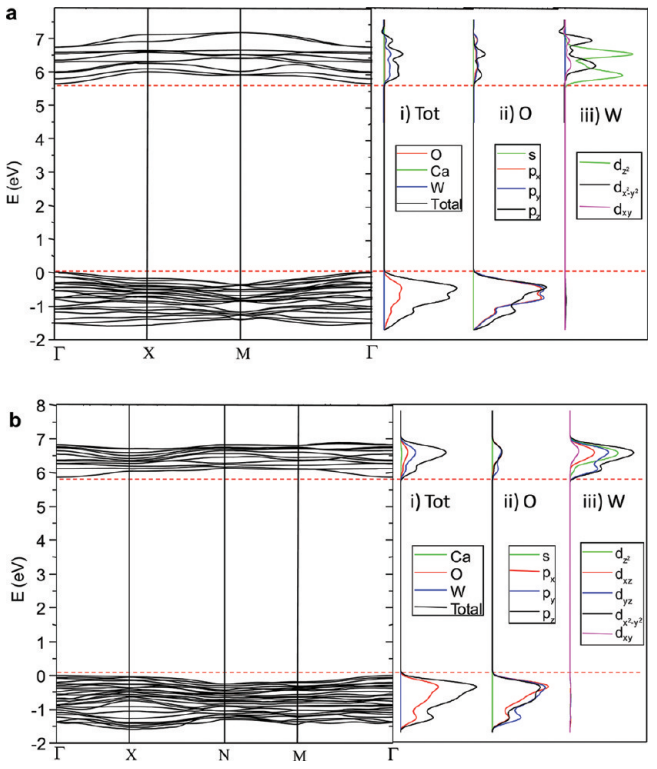

Figure 6. Calculated band structures and density of states for (a) a (001) facet and (b) a (101) facet. The selected *k* points are Γ (000), X (010), M (110), N (100).

aspect is derived mostly from $5d_{z^2}$ with a minor contribution from $5d_{x^2-y^2}$ orbitals of the W atom. On the other hand, in (101) surface, the conduction band presents a mainly $W5d_{x^2-y^2}$ character, which dominates over the $5d_{z^2}$ and $5d_{yz}$ W orbitals. It is apparent that contributions of the O 2p- and W 5d-like states into the valence band (and the conduction band) of calcium tungstate facets depend on the position of these atoms in the corresponding surfaces. As discussed, more than 98% of the total area of the $CaWO_4$ surface comprises the (101) facet that is Ca-terminated.

As many kinds of metal oxides form a wide range of oxygen deficiency intermediate phases,[61−63] it is generally believed that the reconstruction of the metal oxide surface is related to an ordered oxygen vacancy type defect.[63,64] The analysis of different arrangements of Ca and W in (001) and (101) renders diverse degrees of broken chemical bonds on the surface and sites therein. While bonds and coordination in the core interior remain in their bulk nature, that is, WO_4 and CaO_8, in the surface, undercoordinated Ca is found. In (001) surface, Ca is surrounded by six O atoms, three sets of two equivalent distances 2.33, 2.39, and 2.52 Å, respectively. The Ca-terminated (101) surface shows a Ca coordinated to five O atoms at distances of 2.24, 2.26, 2.27, 2.38, and 2.40 Å, respectively. W atoms have a tetrahedral environment in both surfaces more distorted than in bulk, with clearly two different distances, 1.73 and 1.77 Å in (001) surface and 1.71 and 1.79 Å in (101), respectively. The charge analysis is according to this distance value. Therefore, undercoordination at Ca atom can explain the stability order of surface energy between studied surfaces, because the lack of three O atoms in Ca-terminated (101) facets (as well as in (100), (110), and (111)) induces more distortions than the deficiency of two O atoms in O-terminated (001) facets.

5. CONCLUSIONS

The design and synthesis of uniformly sized and morphology-controlled nanostructures have been intensively pursued and well developed in the past years for their sizes and shape-dependent properties. Construction of well-aligned nanostructures with controlled dimensions is critical for practical applications and also for fundamental investigations into the field of new generation nanostructured devices as well as a crystal/assembly growth mechanism. We have focused on these properties in an attempt to highlight the key concepts that are emerging on the basis of the present study.

We have studied the nanomorphology and oriented attachment mechanism for the formation of $CaWO_4$ nanocrystals. To this aim, the combination of experimental techniques such as FEG-SEM, TEM, HRTEM, and first-principle calculations (surface energy) was employed. A thermodynamic model for exploring the relative stability of faceted $CaWO_4$ nanocrystals reveals the morphology and their assembly by an oriented attachment mechanism, while an analysis of the calculated band structures and densities of state elucidates the characterization of the different electronic structure surfaces.

Good agreement between the nanomorphology predicted by theoretical results performed in vacuo with experimental observations can be reached. Changes in the surface energy impact the nanomorphology, and those are sufficient to switch from an attractive to a repulsive situation, that is, the favorable interaction between hydroxyl anions (the synthesis takes place at pH = 10) and Ca atoms of the surface (101).

The proposed theory yields rapid information and is not limited to the system studied. Therefore, this approach could be generalized to overall nanocrystals. The analysis of the surface energy values with experimental figures opens a new avenue in the research for nanocrystal growth and would find various applications in the near future in the field of crystal engineering and materials science.

AUTHOR INFORMATION

Corresponding Authors

*Fax: +55-16-3307-6426 (L.G.); +34 964728066 (J.A.). E-mail: lgracia@qfa.uji.es (L.G.); andres@qfa.uji.es (J.A.).

ACKNOWLEDGMENT

We dedicate this Article to the memory of Dr. Miguel Álvarez Blanco. Financial support is from the Brazilian research funding agencies FAPESP (08/55585-5 and 09/50303-4), CNPq, and FINEP. This work is also supported by Generalitat Valenciana for Prometeo/2009/053 project, Spanish Ministry Ministerio de Ciencia e Innovación for project CTQ2009-14541-C02, Programa de Cooperación Científica con Iberoamerica (Brasil), Ministerio de Educación (PHB2009-0065-PC), Spanish MALTA-Consolider Ingenio 2010 Program (Project CSD2007-00045), and Fundación Bancaja (Project P1 1B2009-08). We acknowledge the Servei dInformatica, Universitat Jaume I, for the generous allotment of computer time.

REFERENCES

(1) Colfen, H.; Mann, S. *Angew. Chem., Int. Ed.* **2003**, *42*, 2350–2365.
(2) Seyed-Razavi, A.; Snook, I. K.; Barnard, A. S. *J. Mater. Chem.* **2010**, *20*, 416–421.

(3) Burda, C.; Chen, X. B.; Narayanan, R.; El-Sayed, M. A. *Chem. Rev.* **2005**, *105*, 1025.
(4) Lovette, M. A.; Browning, A. R.; Griffin, D. W.; Sizemore, J. P.; Snyder, R. C.; Doherty, M. F. *Ind. Eng. Chem. Res.* **2008**, *47*, 9812.
(5) Chen, J. Y.; Lim, B.; Lee, E. P.; Xia, Y. N. *Nano Today* **2009**, *4*, 81.
(6) Lee, K.; Kim, M.; Kim, H. *J. Mater. Chem.* **2010**, *20*, 3791.
(7) Jiang, Z. Y.; Kuang, Q.; Xie, Z. X.; Zheng, L. S. *Adv. Funct. Mater.* **2010**, *20*, 3634.
(8) Gurlo, A. *Nanoscale* **2011**, *3*, 154–165.
(9) Prywer, J. *Prog. Cryst. Growth Charact. Mater.* **2005**, *50*, 1–38.
(10) Barnard, A. S. *Rep. Prog. Phys.* **2010**, *73*, 086502.
(11) Billinge, S. J. L.; Levin, I. *Science* **2007**, *316*, 561–565.
(12) Stroppa, D. G.; Montoro, L. A.; Beltrán, A.; Conti, T. G.; da Silva, R. O.; Andrés, J.; Leite, E. R.; Ramirez, A. J. *Chem. Commun.* **2011**, *47*, 3117–3119.
(13) Stroppa, D. G.; Montoro, L. A.; Beltrán, A.; Conti, T. G.; da Silva, R. O.; Andrés, J.; Longo, E.; Leite, E. R.; Ramirez, A. J. *J. Am. Chem. Soc.* **2009**, *131*, 14544–14548.
(14) Hou, Z. Y.; Li, C. X.; Yang, J.; Lian, H. Z.; Yang, P. P.; Chai, R. T.; Cheng, Z. Y.; Lin, J. *J. Mater. Chem.* **2009**, *19*, 2737–2746.
(15) Chen, Z.; Gong, Q.; Zhu, J.; Yuan, Y. P.; Qian, L. W.; Qian, X. F. *Mater. Res. Bull.* **2009**, *44*, 45–50.
(16) Wang, W. S.; Hu, Y. X.; Goebl, J.; Lu, Z. D.; Zhen, L.; Yin, Y. D. *J. Phys. Chem. C* **2009**, *113*, 16414–16423.
(17) Hernandez-Sanchez, B. A.; Boyle, T. J.; Pratt, H. D.; Rodriguez, M. A.; Brewer, L. N.; Dunphy, D. R. *Chem. Mater.* **2008**, *20*, 6643–6656.
(18) Thongtem, T.; Phuruangrat, A.; Thongtem, S. *Appl. Surf. Sci.* **2008**, *254*, 7581–7585.
(19) Thongtem, T.; Phuruangrat, A.; Thongtem, S. *J. Ceram. Process. Res.* **2008**, *9*, 258–261.
(20) Phuruangrat, A.; Thongtem, T.; Thongtem, S *J. Ceram. Soc. Jpn.* **2008**, *116*, 605–609.
(21) Li, C. X.; Lin, C. K.; Liu, X. M.; Lin, J. *J. Nanosci. Nanotechnol.* **2008**, *8*, 1183–1190.
(22) Wang, Z. L.; Li, G. Z.; Quan, Z. W.; Kong, D. Y.; Liu, X. M.; Yu, M.; Lin, J. *J. Nanosci. Nanotechnol.* **2007**, *7*, 602–609.
(23) Wang, W. S.; Zhen, L.; Xu, C. Y.; Zhang, B. Y.; Shao, W. Z. *J. Nanosci. Nanotechnol.* **2008**, *8*, 1288–1294.
(24) Ryu, J. H.; Yoon, J. W.; Lim, C. S.; Oh, W. C.; Shim, K. B. *Ceram. Int.* **2005**, *31*, 883–888.
(25) Yoshimura, M. *J. Mater. Sci.* **2006**, *41*, 1299–1306.
(26) Sun, L. N.; Cao, M. H.; Wang, Y. H.; Sun, G. B.; Hu, C. W. *J. Cryst. Growth* **2006**, *289*, 231–235.
(27) Wang, Y. G.; Ma, J. F.; Tao, J. T.; Zhu, X. Y.; Zhou, J.; Zhao, Z. Q.; Xie, L. J.; Tian, H. *Mater. Lett.* **2006**, *60*, 291–293.
(28) Chen, S. J.; Li, J.; Chen, X. T.; Hong, J. M.; Xue, Z. L.; You, X. Z. *J. Cryst. Growth* **2003**, *253*, 361–365.
(29) Polshettiwar, V.; Nadagouda, M. N.; Varma, R. S. *Aust. J. Chem.* **2009**, *62*, 16–26.
(30) Katsuki, H.; Shiraishi, A.; Komarneni, S.; Moon, W. J.; Toh, S.; Kaneko, K. *J. Ceram. Soc. Jpn.* **2004**, *112*, 384.
(31) Moreira, M. L.; Paris, E. C.; do Nascimento, G. S.; Longo, V. M.; Sambrano, J. R.; Mastelaro, V. R.; Bernardi, M. I. B.; Andres, J.; Varela, J. A.; Longo, E. *Acta Mater.* **2009**, *57*, 5174.
(32) Macario, L. R.; Moreira, M. L.; Andrés, J.; Longo, E. *CrystEngComm* **2010**, *12*, 3612–3619.
(33) Volanti, D. P.; Orlandi, M. O.; Andrés, J.; Longo, E. *CrystEngComm* **2010**, *12*, 1696–1699.
(34) Moreira, M. L.; Andrés, J.; Longo, E.; Varela, J. A. *Cryst. Growth Des.* **2008**, *9*, 833–839.
(35) Bilecka, I.; Niederberger, M. *Nanoscale* **2010**, *2*, 1358–1374.
(36) Dovesi, R.; Saunders, V. R.; Roetti, C.; Orlando, R.; Zicovich-Wilson, C. M.; Pascale, Doll, K.; Harrison, N. M.; Bush, I. J.; D'Arco, P.; Llunell, M. *CRYSTAL06*; University of Torino: Torino, 2006.
(37) http://www.crystal.unito.it/BasisSets/Ptable.html.
(38) Becke, A. D. *J. Chem. Phys.* **1993**, *98*, 5648–5652.
(39) Lee, C. T.; Yang, W. T.; Parr, R. G. *Phys. Rev. B* **1988**, *37*, 785–789.
(40) Wulff, G. *Z. Krystallogr. Mineral.* **1901**, *34*, 449.
(41) Pimpinelli, A.; Villain, J. *Physics of Crystal Growth*; Cambridge University Press: Cambridge, 1998.
(42) Herring, C. *Phys. Rev.* **1951**, *82*, 87–93.
(43) Sun, C. Q. *Prog. Mater Sci.* **2009**, *54*, 179.
(44) Sun, C. Q. *Prog. Solid State Chem.* **2009**, *35*, 1.
(45) Sun, C. Q. *Nanoscale* **2010**, *2*, 1930.
(46) Liu, X. J.; Li, J. W.; Zhou, Z. F.; Yang, L. W.; Ma, Z. S.; Xie, G. F.; Pan, Y.; Sun, C. Q. *Appl. Phys. Lett.* **2009**, *94*, 131902.
(47) Marks, L. D. *J. Cryst. Growth* **1983**, *61*, 556–566.
(48) Gracia, L.; Beltrán, A.; Andrés, J. *J. Phys. Chem. B* **2006**, *110*, 23417.
(49) Gong, Q.; Qian, X. F.; Ma, X. D.; Zhu, Z. K. *Cryst. Growth Des.* **2006**, *6*, 1821–1825.
(50) Liu, J. P.; Huang, X. T.; Li, Y. Y.; Li, Z. K. *J. Mater. Chem.* **2007**, *17*, 2754–2758.
(51) Zhou, G. J.; Lu, M. K.; Gu, F.; Xu, D.; Yuan, D. R. *J. Cryst. Growth* **2005**, *276*, 577–582.
(52) Zhou, G. J.; Lu, M. K.; Xiu, X. L.; Wang, S. F.; Zhang, H. P.; Zou, W. G. *J. Cryst. Growth* **2005**, *276*, 116–120.
(53) Hu, X. L.; Zhu, Y. J. *Langmuir* **2004**, *20*, 1521–1523.
(54) Zeng, H. C. *Int. J. Nanotechnol.* **2007**, *4*, 329–346.
(55) Ribeiro, C.; Lee, E. J. H.; Longo, E.; Leite, E. R. *ChemPhysChem* **2005**, *6*, 690–696.
(56) Penn, R. L. *J. Phys. Chem. B* **2004**, *108*, 12707–12712.
(57) Xu, X.; Liu, F.; Yu, K.; Huang, W.; Peng, B.; Wei, W. *ChemPhysChem* **2007**, *8*, 703.
(58) Cooper, T. G.; de Leeuw, N. H. *Surf. Sci.* **2003**, *531*, 159–176.
(59) Barnard, A. S.; Curtiss, L. A. *Nano Lett.* **2005**, *5*, 1261.
(60) Barnard, A. S. *Cryst. Growth Des.* **2009**, *9*, 4860–4863.
(61) Rao, C. N. R.; Raveau, B. *Transition Metal Oxides*; VCH: New York, 1995.
(62) Henrich, V. E.; Cox, P. A. *The Surface Science of Metal Oxides*; Cambridge University Press: New York, 1994.
(63) Tanaka, H.; Matsumoto, T.; Kawai, T.; Kawai, S. *Jpn. J. Appl. Phys., Part 1* **1993**, *32*, 1405–1409.
(64) Kubo, T.; Nozoye, H. *Surf. Sci.* **2003**, *542*, 177–191.